Acta Polytechnica **64**(5):398–406, 2024
https://doi.org/10.14311/AP.2024.64.0398

Published by the Czech Technical University in Prague

THE EFFECT OF THE INLET CHAMBER AND DIFFUSER ON THE REVERSE AERODYNAMIC PERFORMANCE OF AN AXIAL FLOW FAN

Václav Cyrus[a,b,*], Jan Cyrus[a]

[a] *AHT Energetika, Štětínská 15, 180 00 Prague, Czech Republic*

[b] *Czech Technical University in Prague, Faculty of Mechanical Engineering, Department of Energy, Jugoslávských partyzánů 3, 160 00 Prague, Czech Republic*

[*] corresponding author: cyrus.aht@iol.cz

Abstract. Flow reversal in axial fans is usually carried out by changing the direction of rotation of the fan and rotating the stator vanes. The total pressure losses of selected inlet fan chambers were determined using CFD data for the normal and reverse flow conditions. These losses are 3.5 to 7.2 times greater for the normal flow increase due to the flow reversal in three chambers with the hub/tip ratio of 0.45 to 0.63. The operating points of two complete fans made up of the inlet chamber, the diffuser, and the axial stages A and B with different aerodynamic load were obtained using one-dimensional engineering calculation method. It uses the measured performance data relating to both fan stages. The calculated volumetric flow rate ratio for reverse and normal operation is 0.68 and 0.55, respectively, for the complete axial fan with the stages A and B. The acquired results are in accordance with the customers' requirements.

Keywords: Axial flow fan, reversing, inlet chamber, performance, simulation.

1. Introduction

Change of the flow direction is often required in emergency situations, in road tunnels, coal mine ventilation, and in a number of chemical plant production lines where the axial flow fans are used. They consist of the inlet chamber (IC), the rotor blade row (R), the inlet guide vane (IGV), the stator vane rows (S), and the outlet diffuser (D); see to Figure 1. Reverse flow is most commonly achieved by changing the direction of rotation of the fan and rotating the stator vanes.

The required reverse volume flow rate Q_{rev} is typically at least 50 % to 60 % of the design operating condition Q_n. The stage blading (IGV, rotor and stator rows) efficiency $\eta_{\mathrm{ST,max}}$ should be higher than $\eta_{\mathrm{ST,max}} = 89\,\%$ to 90 % for standard fan operation. The fan efficiency η_{rev} is usually not specified for the emergency situations. There are only a few works in the literature, namely by Brusilovskij [1],Wallis [2] and Dunn et al. [3], which give brief information on the special reverse axial flow fans. The contribution to the understanding of the flow mechanism in the blade system, based on the investigation data relating to three stages of the reverse axial flow fans, can be found in the works of Cyrus et al. [4], [5].

Our paper presents design study of the complete reverse axial flow fan (IC+IGV+R+S+D) where the directional change of fan rotation and turning of the stator vanes occurs. If the standard axial fan stage is used in the reverse axial fan design then the modified stator vanes must be used in order to meet the condition of the stator vanes being able to turn in one go. In paper by Cyrus et al. [6], the design of new stator vanes for the reverse fans is carried out using the flow simulation results.

Abdolmaleki et al. [7] analysed the aerodynamic performance of two-dimensional cascades with elliptical profiles for isolated rotor blade rows of an axial flow fan. The results were obtained using CFD simulations. Flow reversal is achieved by changing the direction of the fan rotation. The new concept of the axial flow fan stage is described in the publication by Krasyuk et al. [8]. It consists of rotor blades and inlet guide vane rows. During fan reversal, the rotation of the rotor blade row is stopped. The rotation of the inlet guide vane row has then started. This procedure helped to increase the efficiency of the fan during flow reversal.

During civil aircraft landings, the thrust of the turbofan engine can be reduced by rotating the rotor blades of the axial flow fan. The core multistage axial compressor operates unchanged. This approach can produce a reverse flow in the axial flow fan as described in design studies such as [9], [10]. They show the calculated flow fields at selected fan operating points. Some suggestions for a new approach to the aerodynamic design of fan blades are also given.

The new results of the last cited papers cannot be applied in our proposed investigations. In fact, the effort is concentrated on the complete axial fan, where the flow reversal is achieved by changing the direction of rotation of the fan and rotating the stator blades.

In order to determine the complete reverse axial fan aerodynamic performance, the inlet chamber pressure losses data for the normal and reverse fan flow directions are required. Our focus is primarily on the

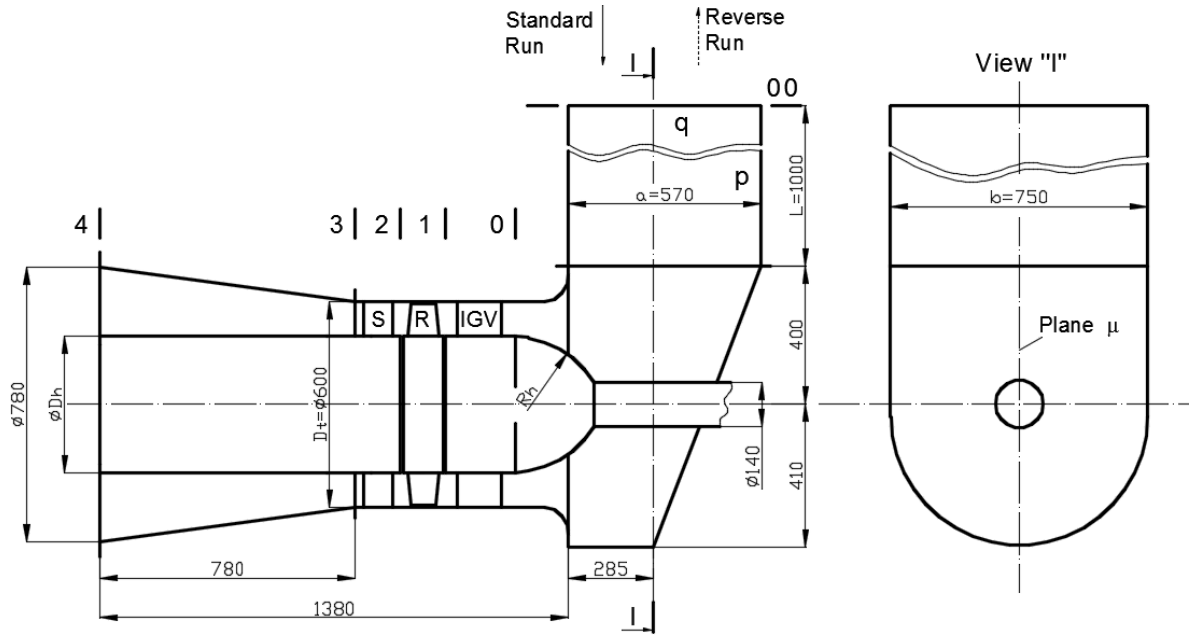

FIGURE 1. Axial flow fan (Stage A: $D_t = 600\,\text{mm}$, $D_h = 330\,\text{mm}$).

Stage	Design parameters											
	φ_D	ψ_D	$\mathbf{DF}_{R,m}$	ν	z_R	z_S	$v_{R,m}$ [°]	$v_{S,m}$ [°]	$\left(\frac{s}{c}\right)_{S,m}$	$\left(\frac{s}{c}\right)_{S,h}$	$\frac{\varphi_{\text{rev}}}{\varphi}$ *	$\frac{\varphi_{\text{rev}}}{\varphi}$ **
A	0.40	0.30	0.36	0.55	12	15	19.5	45.0	1.36	0.86	0.77	0.81
B	0.35	0.42	0.48	0.63	16	17	24.6	51.1	1.20	0.56	0.61	-

* IGV+R+S configuration.

** R+S configuration.

TABLE 1. Fan stages design parameters.

inlet chamber, where the inlet flow velocity vector is perpendicular to the fan axis (Figure 1). New results were obtained using the commercial CFD code Numeca [11] for the inlet chamber with rectangular inlet sides with the ratio of $\frac{b}{a} = 1.32$; see Figure 1. Three hub/tip ratios: $\nu = 0.45$, 0.55, and 0.63 were investigated.

The last part of our paper presents the evaluation of the key parameters, namely the fan reversibility, the flow rate ratio $\frac{Q_{\text{rev}}}{Q}$. It has been determined for two complete fans with the axial flow stages A, B [4] and [5]. The fan performance maps of the specified fan stages practically cover the customers' requirements in the mining and chemical industries. Our calculation is based on the simple one-dimensional engineering calculation method using the theoretical and test stage performance curves. The total pressure losses of the inlet chamber, diffuser, and confuser for standard and reverse fan operation have been applied. The results obtained will allow the fan designer to assess the effect of individual components of the complete fan on its aerodynamic performance during standard and reverse fan operation.

2. Axial flow stages for reverse fans

Our paper analyses the data relating to the two axial fan flow stages, denoted A and B, designed at AHT Energetika Ltd. with the aid of in-house design code designated for the axial flow compressor stages. The key fan stage parameters, namely the flow coefficient φ, the pressure coefficient ψ, and the efficiency η are defined as follows:

$$\varphi = \frac{Q}{Au_t}, \tag{1}$$

$$\psi = 2\frac{\Delta p_T}{\rho u_t^2}, \tag{2}$$

$$\eta = Q\frac{\Delta p_T}{P}. \tag{3}$$

Selected key aerodynamic and geometric parameters are given in Table 1. A is the flow area $A = \pi D_t^2 \frac{1-\nu^2}{4}$; u_t is the peripheral velocity; Δp_T is the total pressure increment in the fan stage $\Delta p_T = p_{T3} - p_{T0}$; ρ is the gas density; D_t is the external diameter; ν is the stage hub/tip ratio $\nu = \frac{D_h}{D_t}$ and P is the fan stage work input $P = M_k\omega$. Angular frequency is denoted

by Greek letter ω. The test rig was driven by a DC motor with a swinging stator in order to measure the torque moment M_k by weighing. Equation (3) can be derived from the definition of the isentropic efficiency of a turbo-compressor, e.g. [12]. Here, the compressibility of the air is taken into account.

Stages A and B have moderate aerodynamic load, which is suitable for designing a larger number of ventilation fans. The blade geometry is given at the mean radius r_m ($r_m = 0.5(r_t + r_h)$). The stage parameters φ and ψ are defined by the Equations (1) and (2), respectively. The symbol z denotes the number of blades. The cascade profile camber υ is given by the following relationship: $\upsilon = \beta_{L1} - \beta_{L2}$, where β_{L1} and β_{L2} are the blade angles (Figure 2) that the entry and exit tangents to the camber line make with the axial direction. $\mathrm{DF}_{R,m}$ is the design diffusion factor of the rotor blades on the mean radius, originally formulated by Lieblein [13]. The cascades of stages A and B have the rotor diffusion factor at the mean radius of $\mathrm{DF}_{R,m} = 0.36$ and 0.48, respectively. The external diameters of the tested fan stages were the same: $D_t = 600\,\mathrm{mm}$ (Figure 1).

The rotor and stator profiles for all stages were NACA 65 series with reinforced trailing edge and circular camber lines. The profile coordinates can be found, for example, in [2], [12]. The stage B had curved plate stator vanes. The blades of all tested axial stages were designed assuming the uniform spanwise work distribution. Near the rotor blade axis, the ratio of tip clearance and chord length $\frac{s_r}{c_t}$ was 0.008.

The tests were carried out on fan stages A and B at revolutions of 2 200 and 1 500 rpm, respectively. The inlet flow Mach number lower than $\mathrm{Ma}_1 = \frac{w_1}{a} < 0.35$. a is sonic velocity. The air compressibility can be neglected. The Reynolds number values $\mathrm{Re} = u_t \frac{c_{R,m}}{\nu}$ ranged from 300 000 to 450 000, where ν is the kinematic viscosity of the air and $c_{R,m}$ is the chord length of the rotor blade at midspan.

Detailed flow field investigations in planes 0, 1, 2 and 3 (Figure 1) were carried out using 5-hole conical pressure probes with a sensor diameter of 2.5 mm. The pressure probes were located at 6 to 11 radial positions and the stator vanes pitch at 15 to 20 circumferential points. Thermocouples were fitted in planes 0 and 2 at the midspan. This measurement technique was used for the stage A. In the case of the stage B, the pressure probes were only in planes 0 and 3. The flow parameters acquired from the pressure probes and thermocouple data were averaged over the vane pitch. The fan stage performance curves' points were calculated using the averages of the flow properties in the inlet and outlet planes of the tested stage.

The absolute measurement uncertainty of the stage efficiency was calculated as ±0.9 % to ±1.1 % at the design point. Measurement errors of the following properties were considered in the uncertainty analysis: pressure ±5 Pa, temperature ±0.3 K, flow angle ±1°, torque ±0.08 Nm.

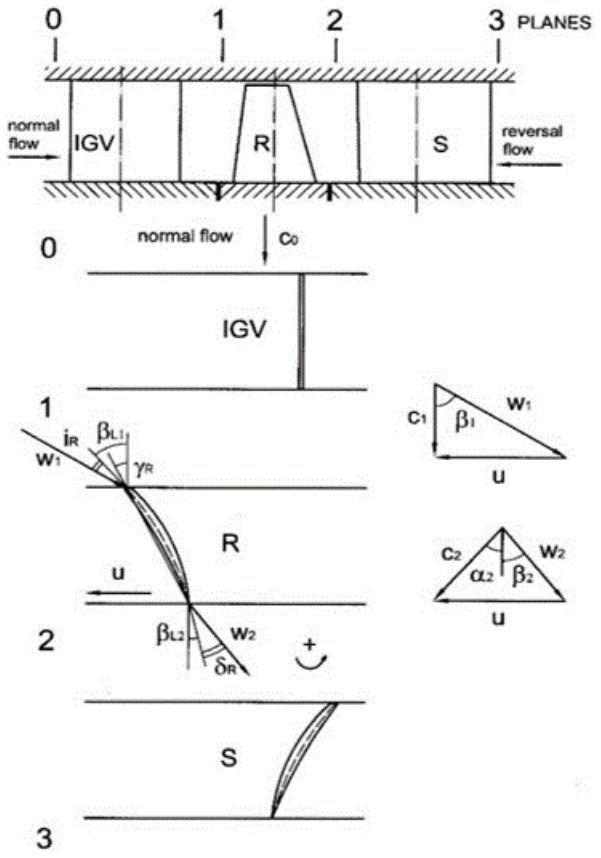

Figure 2. Axial flow fan stage diagrams with velocity triangles: standard flow.

3. Flow description in the fan stage blades during reverse operation

Figures 2 and 3 show 2D basic fan stage cascades together with the velocity triangles valid for the standard and reverse runs. Firstly, we consider the operating condition for the rotor blade row cascades during the fan stage reversal [4].

By changing the rotor blade row direction of a rotation, the compressor-type cascade becomes the turbine-type cascade. For the compressor work, during the rotor blades reverse operation, the relationship is valid for the relative flow angles (Figure 3):

$$\beta'_2 > \beta'_1. \tag{4}$$

By introducing the incidence angle i'_R and the flow deviation δ'_R inequality (4), it changes to:

$$\beta_{L2,R} + i'_R > \beta_{L1,R} - \delta'_R, \tag{5}$$

where $\beta_{L1,R}$ and $\beta_{L2,R}$ are the rotor blade angles. Simplifying, we arrive at:

$$i'_R > k\upsilon_R, \quad \upsilon_R = \beta_{L1,R} - \beta_{L2,R}, \tag{6}$$

where the constant k can be within the range of $k = 0.60$ to 0.85 for the standard cascade parameters [4]. The condition (6) shows that the required

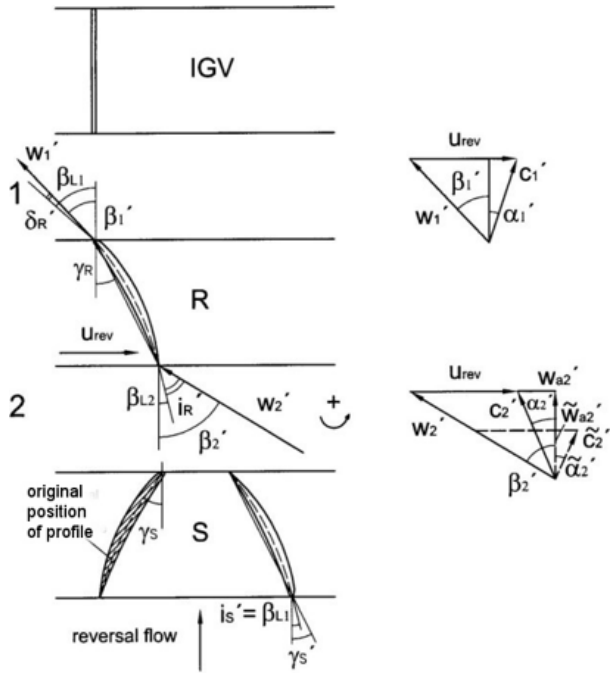

FIGURE 3. Axial flow fan stage diagrams with velocity triangles: reverse flow.

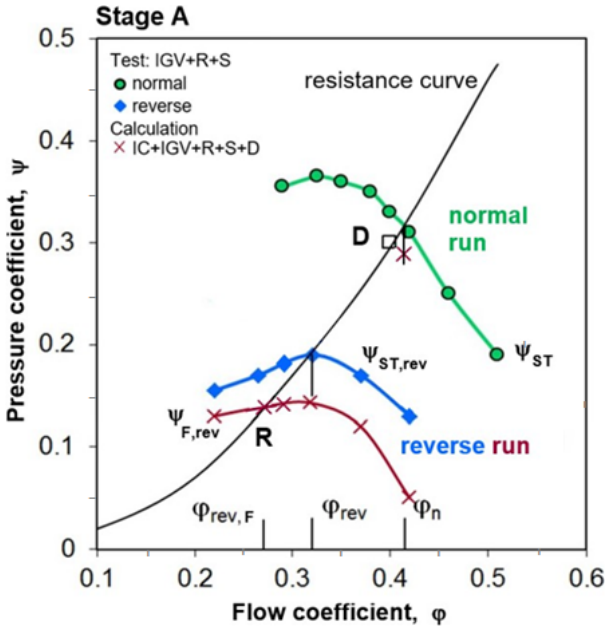

FIGURE 4. Relationship between the pressure coefficient and the flow coefficient for stage A and the complete fan during the standard and reverse flow.

rotor row i'_R incidence angle, essential for achieving the compressor cascade regime, increases with the blade profile camber υ_R. During the flow reversal, the stator vanes are rearranged in the opposite sense of the stagger angle γ_S in relation to the original position. This step follows from the velocity triangle in plane 2 (Figure 3). In order to achieve the same relative flow angle β'_2, and therefore the same incidence angle of rotor row i'_R, the axial velocity component $\widetilde{w}'_{a2}$ would have to be significantly reduced, as shown by the velocity triangle. The original setting of the stator blade has been retained. However, this is not desired, as it increases the gap between the performance lines for the standard and reverse operation [1], [4], [5].

4. Performance of fan stages A and B (IGV+R+S) during standard and reverse operation

Comparisons of the fan stage A measured pressure coefficient ψ, the efficiency η, and the flow coefficient φ for the standard and reverse operation are shown in Figures 4 and 5. The stator vanes were set to the stagger angle $\gamma_S = -10°$ at flow reversal. The resistance graph shown in Figure 4 intersects the design point D. The ratio of the flow coefficients was found to be $\frac{\varphi_{rev}}{\varphi_n} = 0.77$. For the fan stage B, this ratio is lower $\frac{\varphi_{rev}}{\varphi_n} = 0.62$ owing to the higher aerodynamic loading of the rotor blade elements; see to Table 1.

It is apparent that in the fan stage, the reverse flow parameter $\frac{\varphi_{rev}}{\varphi_n}$ ($\frac{Q_{rev}}{Q}$) decreases with the increasing aerodynamic loading of the rotor blade elements. It relates to the increased blade profile camber υ_R.

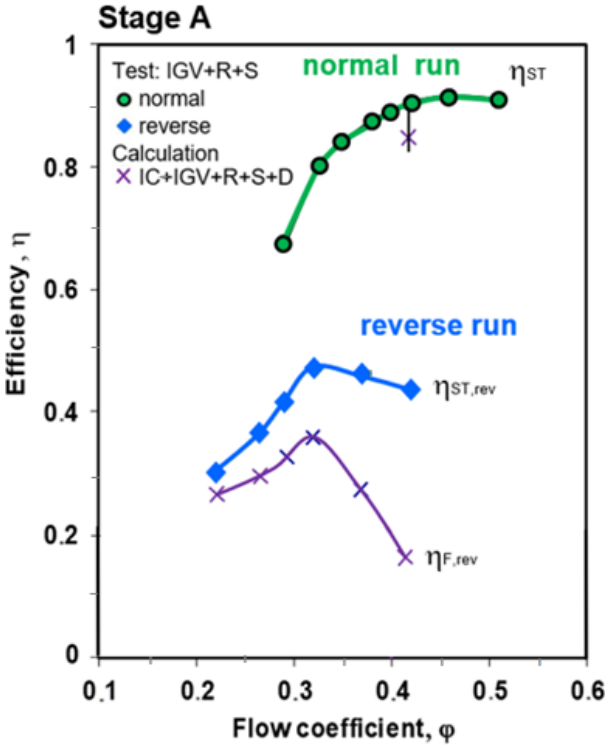

FIGURE 5. Relationship between the efficiency and the flow coefficient for stage A and the complete fan during the standard and reverse flow.

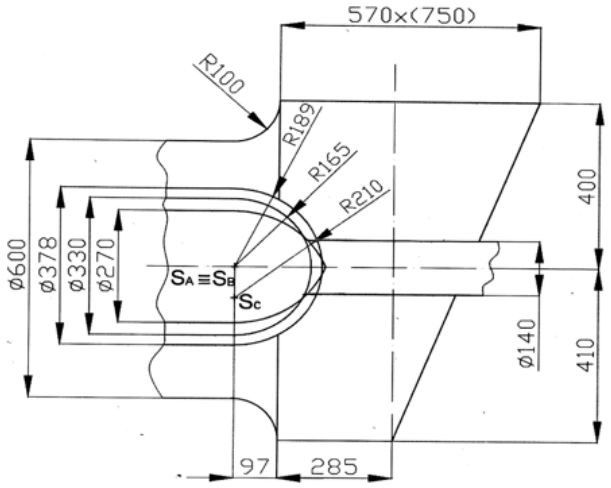

Figure 6. Inlet chambers for fan hub/tip ratios: $\nu = 0.45$, 0.55 and 0.63; $D_h = 270$ mm, 330 mm and 378 mm.

5. Inlet chamber pressure losses during the normal and reverse flow

5.1. CFD simulations of the inlet chamber

A detailed flow analysis of the complete axial fan was carried out using CFD flow simulations [11] and test results, [5], [14] over a wide operating range at standard fan operation. The 3D flow in the outlet diffuser and inlet chamber was also studied, particularly at off-design conditions. The results obtained are compatible with published data, e.g. [15], [12].

Data relating to the inlet chamber reverse flow pressure losses are not available in the relevant literature. For this reason, the study was carried out on one type of chamber in the range of hub/tip ratios $\nu = 0.45$ to 0.70. The relative geometric parameter of the inlet rectangular area was: $\frac{b}{a} = 1.32$ (Figure 1). The comparison of three flow channels of the inlet chamber with different hubs is shown in Figure 6. The hub/tip ratio values were $\nu = 0.55$, 0.63, and 0.45. The first two hub variants are formed by parts of a hemisphere, the last one by a part of an ellipsoid.

CFD simulations were performed using the CFD commercial code Numeca [11] in the inlet chamber with the rectangular inlet duct $\frac{L}{D_t} = 1.67$ (Figure 1, relative distance of the planes) for the standard and reverse flow directions. The commercial code solved the full Reynolds-averaged Navier Stokes equations for the structure multi-block arbitrary grid topologies. Hexadron cells were used. The explicit time marching 4 steps Runge-Kutta procedure with the implicit residuum smoothing was used. A cell centred second order finite volume discretisation was applied. The cell width, at walls, was kept in the range of 0.03 to 0.07 mm in all cases to ensure that the wall y^+ did not exceed 5. The air was modelled as a perfect gas. A no-slip boundary condition was imposed on the walls. The Spallart-Almaras turbulence model was applied.

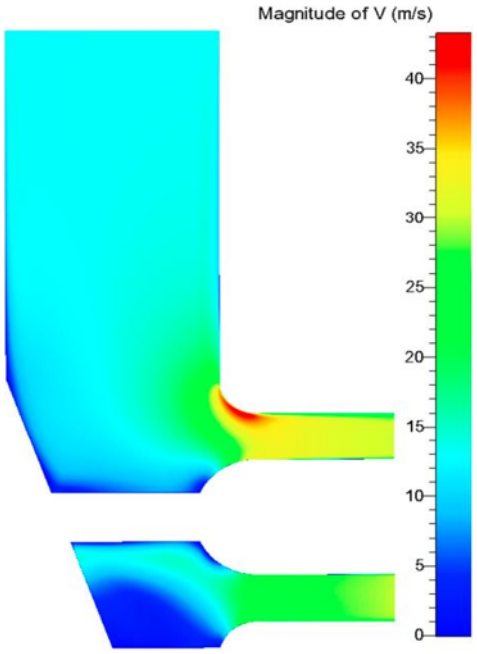

Figure 7. Flow velocity contours in the fan inlet chamber's vertical symmetry plane during the standard flow ($\nu = 0.55$).

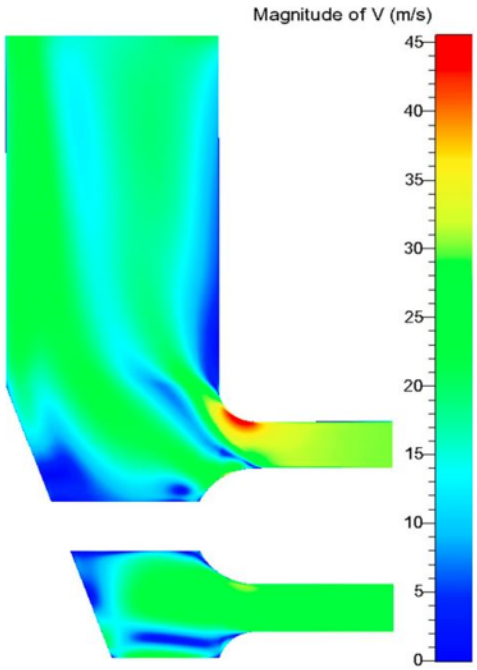

Figure 8. Flow velocity contours in the fan inlet chamber's vertical symmetry plane during the reverse flow ($\nu = 0.55$).

To take advantage of the lateral symmetry of the domain, only half of the chamber section was modelled, see Figures 7, 8, and 9. The position of the meridional symmetry plane μ can be seen in Figures 1 and 9. It is defined by the straight lines p and q. By imposing the symmetry condition on the surface of the plane μ, zero shear is obtained.

The computational grid consisted of 2.5 million cells, distributed over three main sections of the domain: the rectangular inlet duct, the box and the annular section. The number of cells was chosen according to rules published in the literature, e.g. [11], based on CFD results. These data were obtained for the cell number in the range of 1.0 to 3.5 million.

The flow turbulent and laminar viscosity ratio $\frac{\nu_T}{\nu_L} = 6.5$ was used in the turbulence model at the inlet chamber's inlet plane. This is appropriate for the turbulent flow behind the fan blades.

The convergence was evaluated through a computation of residuals, which, at the end of calculations, were of the order of 10^{-6}.

The inlet flow conditions were modelled in the CFD simulations according to the Stage A test results. For the normal fan operation, the inlet flow angle in plane 00 was zero: $\alpha_0 = 0°$. The spanwise distribution of total pressure p_T and flow angle α_0 in the chamber inlet plane 1 was used for the flow reversal. These data refer to experimental results obtained for operating points in the range of flow coefficient $\varphi_{\text{rev}} = 0.22$ to 0.41 (Figure 4). The spanwise distributions of the angles are in the range of values $\alpha_0 = -7°$ to $+7°$ for the relative blade height $\frac{z}{h} = 0$ to 0.8.

5.2. CFD RESULTS AND THEIR ANALYSIS

The comparison of the total pressure losses given by the loss coefficients at the standard ζ_{IC} and the reverse flow directions $\zeta_{\text{IC,rev}}$ is shown in Table 2 for three hub/tip ratios: ($\nu = 0.45$, 0.55, and 0.63). Definitions of loss coefficients ζ_{IC} are as follows:

$$\begin{aligned} \zeta_{\text{IC}} &= \frac{p_{T00} - p_{T0}}{q_1} \quad \text{standard flow,} \\ \zeta_{\text{IC,rev}} &= \frac{p_{T0} - p_{T00}}{q_1} \quad \text{reverse flow,} \\ q_1 &= 0.5\rho(\frac{Q}{A})^2. \end{aligned} \tag{7}$$

Table 2 shows that the loss coefficient $\zeta_{\text{IC,rev}}$ increases with increasing hub/tip ratio ν. It is related to the increasing area ratio $\frac{A_{00}}{A_0}$ in the range of $\frac{A_{00}}{A_0} = 1.9$ to 2.5. This tendency causes the growth of the separated flow areas on the surfaces of the inlet chamber flow channels. At the lowest value of ratio $\nu = 0.45$, the loss coefficient $\zeta_{\text{IC,rev}}$ is significantly lower $\zeta_{\text{IC,rev}} = 0.265$ than in the cases of hub/tip ratios $\nu = 0.55$ and 0.63: $\zeta_{\text{IC,rev}} = 0.45$ and 0.501, respectively. This can be explained by lower flow diffusion in the inlet chamber at flow reversal. Inlet flow angle $\alpha_0 = 0°$ was considered in comparisons.

The effect of the inlet flow angle of the chamber α_0 on total pressure loss coefficient $\zeta_{\text{IC,rev}}$ was investigated for three constant spanwise distributions at three typical values of $\alpha_0 = 0°$, -7°, +7°. It is apparent that the differences are not significant. Figures 7 and 8 compare the contours of the constant flow velocity of the inlet chamber symmetry plane µ during the normal and reverse flow. The computed flow patterns

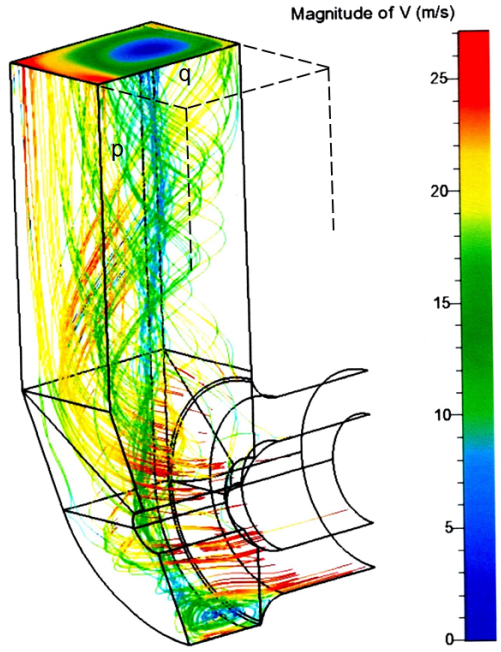

FIGURE 9. 3D flow streamlines in the half of fan inlet chamber and the inlet piping during the reverse flow ($\nu = 0.55$).

ν	$\frac{A_{00}}{A_0}$	$\zeta_{\text{IC,rev}}$	α_0 [°]	$\frac{\zeta_{\text{IC,rev}}}{\zeta_{\text{IC}}}$
0.45	1.90	0.246	0	3.5
0.55	2.16	0.467	0	6.8
		0.500	0	7.2
0.63	2.5	0.452	−7	
		0.492	7	

TABLE 2. Pressure losses in the inlet chamber.

are valid for the hub/tip ratio of $\nu = 0.55$ and a flow angle of $\alpha_0 = 0°$.

The Reynolds number Re = 124 200 ($\text{Re} = w_1\frac{h}{\nu}$) was for the normal flow in our fan; h is the annulus height, $h = 0.5(D_t - D_h)$. The inlet flow conditions refer to the design point of fan stage A ($\varphi_n = 0.40$).

The flow is separated on the hub and the outer annular surface of the inlet chamber due to relatively high flow diffusion. The area ratio $\frac{A_{00}}{A_0}$ is 2.16. The vortex structure of the separated flow is shed and transported in the direction of the flow on spiral streamlines as shown in Figure 9 ($\alpha = 0°$). Here, the complex 3D flow in one half of the inlet chamber is displayed. The streamlines' colour is derived from flow velocity values. In the outlet plane 00 with a rectangular shape, there are two counter-rotating vortices. In their centre (core), the streamlines with a relatively low velocity ($V < 9\,\text{m}\,\text{s}^{-1}$) are concentrated. Figure 9 shows only one vortex due to the flow symmetry to the vertical meridional plane µ. The division of the vortex into two branches takes place at the chamber bottom.

The relatively high total pressure losses of the inlet chamber were evaluated, as can be found in Table 2. The flow energy losses in turbomachinery chambers and diffusers are often divided into friction and mixing losses. In our case of the reverse fan operation, the total pressure losses were mainly caused by flow mixing. This phenomenon occurs after the sudden enlargement of the flow area in the inlet chamber during flow reversal. This is a standard example of thermodynamically irreversible process. The conservation of mass and momentum allows the rise in static pressure and the fall in total pressure. The total pressure friction losses are apparently lower, as can be seen from Figures 8 and 9. The flow around chamber surfaces often exhibits separation. However, during a normal fan operation, the flow is without significant separation on channel surfaces (Figure 7). The mixing energy losses are decreased compared to the case of the fan during flow reversal.

6. The effect of the inlet chamber and the diffuser pressure losses on the overall fan aerodynamic performance during the flow reversal

The complete aerodynamic performance of the axial flow fan is calculated using a one-dimensional flow model. The results, shown in the previous paragraph, relating to the inlet chamber and the diffuser total pressure losses [15], [14] are applied. Our objective is to determine the relationship between the pressure coefficient ψ_F and the flow coefficient φ during the standard and reverse operation for two fans with the stage blading A and B. This is required to determine the flow rates of the fan operating points on the resistance curve of the connected piping system. The same resistance curve is assumed for both flow directions.

The following equation is derived by using the axial flow fan total flow pressure increment $\Delta p_{T,F}$, the stage total pressure increment $\Delta p_{T,\mathrm{ST}}$, and the total pressure losses in the fan inlet $\Delta p_{T,\mathrm{IC}}$ and outlet $\Delta p_{T,D}$ fan sections:

$$\Delta p_{T,F} = \Delta p_{T,\mathrm{ST}} - (\Delta p_{T,\mathrm{IC}} + \Delta p_{T,D}). \qquad (8)$$

By using the definitions of coefficients φ, ψ, and η: (1), (2) and (3), respectively, along with Equation (8), the following relationship can be obtained:

$$\frac{\psi_F}{\psi_{\mathrm{ST}}} = \frac{\eta_F}{\eta_{\mathrm{ST}}} = 1 - (\zeta_{\mathrm{IC}} + \zeta_D)\frac{\varphi^2}{\psi_{\mathrm{ST}}}. \qquad (9)$$

This equation shows that the fan pressure coefficient ψ_F and efficiency η_F decrease due to the energy losses in the inlet chamber and the diffuser $(\zeta_{\mathrm{IC}} + \zeta_D)$ with the increasing flow coefficient φ and the decreasing pressure coefficient ψ_{ST}. The equation reflects the normal and reverse flow.

Definitions of loss coefficients are as follows:

$$\zeta_D = \frac{p_{T3} - p_{T4}}{q_1},$$
$$\zeta_{D,\mathrm{rev}} = \zeta_{\mathrm{con}} = \frac{p_{T4} - p_{T3}}{q_1}, \qquad (10)$$
$$q_1 = q_0 = q_3 = 0.5\rho(\frac{Q}{A})^2.$$

It should be added that the axial fan diffuser acts as a confusor during the reverse flow. The performance of the stage blading (IGV+R+S) during the flow reversal cannot be reliably determined using CFD results due to the origin of large regions of separated flow on the blades' surfaces. This applies to our fan stages A and B. Therefore, we rely on the stage test performance. As mentioned earlier in this paper, the comparison of the dependences of the pressure coefficient ψ and the efficiency η on the flow coefficient φ measured in stage A for normal and reverse flow runs are shown in Figures 4 and 5. The resistance curve shown in the mentioned Figure 4 intersects the performance curve valid for the normal flow at the point with the coordinates: $\varphi_n = 0.415$, $\psi_{\mathrm{ST},n} = 0.31$. During the flow reversal, we get the point with the following coordinates: $\varphi_{\mathrm{rev}} = 0.318$, $\psi_{\mathrm{ST,rev}} = 0.19$. Then, the flow coefficients' ratio is $\frac{\varphi_{\mathrm{rev}}}{\varphi_n} = 0.77$.

The pressure coefficient valid for the reverse flow in the complete fan $\psi_{F,\mathrm{rev}}$ is determined in accordance with the Equation (9). The following relationship is obtained after substitution:

$$\psi_{F,\mathrm{rev}} = \psi_{\mathrm{ST,rev}} - (\zeta_{\mathrm{IC,rev}} + \zeta_{\mathrm{con}})\varphi^2_{\mathrm{rev}}. \qquad (11)$$

Using the data given in Table 2, namely $\zeta_{\mathrm{IC,rev}} = 0.467$ and in Idelchik's work [16], namely $\zeta_{\mathrm{con}} = 0.04$ in Equation (11), the reverse characteristic of the fan is determined (brown crosses). It crosses the resistance curve at the point R with coordinates: $\varphi_{F,\mathrm{rev}} = 0.27$, $\psi_{F,\mathrm{rev}} = 0.139$ (Figure 4).

Again, the complete fan characteristics for the normal flow were determined using Equation (9). After substituting the inlet chamber loss coefficient $\zeta_{\mathrm{IC}} = 0.09$ and the diffuser loss coefficient $\zeta_D = 0.05$, $\varphi_n = 0.41$ and $\psi_{\mathrm{ST},n} = 0.31$, we obtain $\psi_F = 0.286$. The diffuser loss coefficient was determined according to works of Japikse et al. [15] and Cyrus et al. [14].

The desired flow coefficient ratio of $\frac{\varphi_{\mathrm{rev},F}}{\varphi_F} = 0.68$ was achieved based on the calculated results. The complete fan efficiency values can be found in Figure 5: $\eta_F = 0.891$ ($\varphi = 0.41$) and $\eta_{F,\mathrm{rev}} = 0.295$ ($\varphi_{\mathrm{rev}} = 0.27$).

For the fan stage blading B, which has a higher aerodynamic load, the ratio $\frac{\varphi_{\mathrm{rev}}}{\varphi_n}$ is lower, i.e. 0.62; see Table 3. The flow coefficient ratio $\frac{\varphi_{\mathrm{rev},F}}{\varphi_F}$ valid for the complete fan B is only $\frac{\varphi_{\mathrm{rev},F}}{\varphi_F} = 0.55$. The same calculation method was used as for the fan A, as described above.

In order to increase the fan flow ratio $\frac{\varphi_{\mathrm{rev}}}{\varphi_n}$, it is appropriate to reduce the inlet chamber pressure losses

Stage	Stage (IGV+R+S) $\frac{\varphi_{rev}}{\varphi_n}$	Fan (IC+IGV+R+S+D) $\frac{\varphi_{F,rev}}{\varphi_n}$
A	0.77	0.68
B	0.62	0.55

TABLE 3. Ratio of flow rates at reverse and standard operation for stage and fan (A and B).

at flow reversal. The new design concept of the inlet chamber could consist of an extension of its axial length and a reduction of the sides of the rectangle ratio $\frac{b}{a}$.

7. CONCLUSION

This paper summarises the main findings of the aerodynamic phenomena that occur during flow reversal, when the direction of rotation of the axial fan is changed and the stator vanes of the fan are rotated. Our objective was to determine the characteristics of the complete fan, consisting of the inlet chamber, inlet guide vanes, rotor and stator blade rows, and a diffuser, during normal and reverse operation. We also needed to obtain the inlet chamber pressure loss data from the flow simulation results for typical fan hub/tip ratios. The aerodynamic performance of two selected axial flow fans with stages A and B subjected to different aerodynamic loads was then calculated using a one-dimensional flow model. The experimental aerodynamic performance of both stages was used in our study due to an inaccurate CFD performance prediction at flow reversal. The main results of our study are as follows:

(1.) Tests have shown that stages A and B can be used for the flow reversal as the minimum ratio of flow rates is $\frac{\varphi_{rev}}{\varphi_{ST}} = 0.77$ and 0.62, respectively.

(2.) The inlet chamber pressure losses increase at flow reversal was investigated for three hub/tip ratio values : $\nu = 0.45$, 0.55, and 0.63 on the basis of CFD data. As the hub/tip ratio was increased the area ratio increased in the range of $\frac{A_{00}}{A_0} = 1.9$ to 2.5. This tendency causes the growth of the separated flow areas on the surfaces of the inlet chamber flow channels. At the lowest value of ratio $\nu = 0.45$, the loss coefficient $\zeta_{IC,rev}$ is significantly lower $\zeta_{IC,rev} = 0.265$ than in the cases of hub/tip ratios $\nu = 0.55$ and 0.63: $\zeta_{IC,rev} = 0.450$ and 0.501, respectively. This can be explained by lower flow diffusion in the inlet chamber at flow reversal.

(3.) Prediction of the complete axial fan performance is carried out with the use of one-dimensional flow calculation. The inlet chamber and the outlet diffuser pressure losses have a significant impact on the complete reverse fan performance. For the fan A, for example, the fan flow coefficient ratio is reduced from $\frac{\varphi_{ST,rev}}{\varphi_{ST,n}} = 0.77$ valid for the stage to $\frac{\varphi_{F,rev}}{\varphi_{F,n}} = 0.68$ for the complete fan. In terms of efficiency, there will be a drop from $\eta_{ST,rev} = 0.420$ to $\eta_{F,rev} = 0.295$. In the case of the fan with the stage B, the ratio is lower $\frac{\varphi_{F,rev}}{\varphi_{F,n}} = 0.55$. These obtained results meet customer requirements of $\frac{\varphi_{F,rev}}{\varphi_{F,n}} > 0.50$–$0.60$.

(4.) The results of our study will allow the fan designer to assess the effect of individual components of the complete fan on its aerodynamic performance during the standard and reverse fan operation. A further refinement of the calculation method is possible by using the test data of the complete fan model.

LIST OF SYMBOLS

A Flow area [m^2]
c Blade chord [m]
c Absolute flow velocity [$m\,s^{-1}$]
D Diameter [m]
DF Diffusion factor
$DF = 1 - \frac{\cos\alpha_1}{\cos\alpha_2} + 0.5\frac{s}{c}\cos\alpha_1(\tan\alpha_1 - \tan\alpha_2)$
h Height [m]
i Incidence angle [°]
Ma Mach number
M_k Torque [Nm]
P Fan input [W]
p Pressure [Pa]
Q Volume flow rate [$m^3\,s^{-1}$]
r Radius [m]
s Blade spacing [m]
u Peripheral velocity [$m\,s^{-1}$]
w Flow velocity [$m\,s^{-1}$]
z Blades number
α Absolute flow angle [°]
β Relative flow angle [°]
β_L Blade angle [°]
γ Blade stagger angle [°]
ζ Loss coefficient
η Efficiency
υ Camber angle [°]
μ Plane of symmetry
ν Hub/tip ratio
ρ Density [$kg\,m^{-3}$]
φ Flow coefficient
ψ Pressure coefficient
ω Angular frequency [s^{-1}]

Indexes

D Design
D Diffuser
F Fan
h Hub
IC Inlet casing
IGV Inlet guide vanes
m Mean
n Normal

rev Reverse
R Rotor
S Stator
ST Stage
t Tip
T Total
1 Inlet
2 Outlet
$0, 1, 2, 3$ Planes of stage
$()'$ Reverse

Acknowledgements

Our study was carried out for ZVVZ Machinery and was supported by a grant from the Czech Technology Agency (TACR, TA04020228) and a grant from the Czech Ministry of Trade and Industry (TIP FR-TI1/347). The authors were pleased to receive these grants and would like to express their gratitude.

References

[1] I. J. Brusilovskij. *Aerodinamiceskij rascot osevych ventilatorov [In Russian; Aerodynamic design of axial fans].* Mashinostrojenije, Moscow, Russia, 1986.

[2] R. A. Wallis. *Axial flow fans & ducts.* John Wiley & Sons, New York, USA, 1983.

[3] M. F. Dunn, F. S. Kendorski, S. Bhattacharya, et al. Reverse performance characteristics of main mine fans. *Mining Science and Technology* **1**(1):59–68, 1983. https://doi.org/10.1016/S0167-9031(83)90132-9

[4] V. Cyrus. Axial fan at reversal flow. In *Proceedings of the American Society of Mechanical Engineers Turbo Expo 2004*, vol. 5, pp. 437–446. 2004. https://doi.org/10.1115/GT2004-53446

[5] V. Cyrus, J. Pelnar, J. Cyrus. Reversing of axial flow fans for ventilation. In *Proceedings of the American Society of Mechanical Engineers Turbo Expo 2011*, vol. 4, pp. 471–482. 2011. https://doi.org/10.1115/GT2011-46062

[6] V. Cyrus, J. Cyrus. Design study to axial flow fan stator blade row used in reverse ventilation. In *Proceedings of International Conference FAN 2018*, p. 30. 2018.

[7] M. Abdolmaleki, H. Afshin, B. Farhanieh. Performance analysis of elliptic-profile airfoil cascade for designing reversible axial flow fans. *AIAA Journal* **57**(4):1492–1501, 2019. https://doi.org/10.2514/1.J057843

[8] M. J. Krasyuk, P. V. Kosygh. Reversivnyj osevoj ventiljator, aerodinamiceskaja schema ventiljatora, sposob reversirovanija, vrascajuscijsa napravljajuscij apparat [In Russian; Aerodynamic design of axial fan with guide vane for reverse air flow]. *Fyziko-techniceskije problemy razrabotky poleznych iskopaemych* **59**(3):85–95, 2023. https://doi.org/10.15372/FTPRPI20230309

[9] T. S. Williams, C. A. Hall. Reverse thrust aerodynamics of variable pitch fans. *Journal of Turbomachinery* **141**(8):081008, 2019. https://doi.org/10.1115/1.4043139

[10] T. S. Williams, C. A. Hall, M. Wilson. Variable pitch fan aerodynamic design for reverse thrust operation. *Journal of the Global Power and Propulsion Society* **7**:127–139, 2023. https://doi.org/10.33737/jgpps/160096

[11] Numeca International. FINE^{TM} Turbo Numeca code, 2017.

[12] N. A. Cumpsty. *Compressor aerodynamics.* Krieger publishing Company, Florida, USA, 2004.

[13] S. Lieblein. *The Aerodynamic Design of Axial Flow Compressor*, chap. VI. Experimental flow in two-dimensional cascades. NASA, 1966. Reprinted NASA SP 36 in 1965, originally NACA RME 56B03.

[14] V. Cyrus, J. Cyrus, P. Wurst, P. Panek. Aerodynamic performance of advanced axial flow fan for power industry within its operational range. In *Proceedings of the American Society of Mechanical Engineers Turbo Expo 2014*, vol. 1A, p. V01AT10A006. 2014. https://doi.org/10.1115/GT2014-25339

[15] D. Japikse, N. C. Baines. *Diffuser design technology.* Concepts ETI, Vermont, USA, 1998.

[16] I. E. Idelchik. *Handbook of hydraulic resistance.* Jaico Publishing House, Delhi, India, 3rd edn., 2003.